

Effects of preorganization in the chelation of UO_2^{2+} by hydroxamate ligands: cyclic PIPO⁻ vs linear NMA⁻

Alejandra Sornosa-Ten,^a Paweł Jewula,^a Tamas Fodor,^a Stéphane Brandès,^a Vladimir Sladkov,^b Yoann Rousselin,^a Christine Stern,^a Jean-Claude Chambron^{*a} and Michel Meyer^{*a}

^a Institut de Chimie Moléculaire de l'Université de Bourgogne (ICMUB), UMR 6302, CNRS, Université de Bourgogne–Franche-Comté, 9 avenue Alain Savary, BP 47870, 21078 Dijon Cedex, France

^b Institut de Physique Nucléaire d'Orsay (IPNO), UMR 8608, CNRS, Université Paris Sud, 15 rue George Clemenceau, 91406 Orsay Cedex, France

Supporting Information

Contents

I.	Crystallographic data for $[\text{UO}_2(\text{PIPO})_2(\text{H}_2\text{O})]$	3
II.	X-ray powder diffraction studies of uranyl complexes	7
III.	Spectroscopic data of uranyl complexes	9
1.	Diffuse reflectance spectroscopy	9
2.	Infrared spectroscopy	9
3.	Raman spectroscopy	12
IV.	Protonation constants of NMA^-	15
V.	Isothermal titration calorimetric study of the protonation of NMA^- and PIPO^-	16
VI.	Hydrolysis constants of UO_2^{2+}	17
VII.	Affinity capillary electrophoretic study of the $\text{UO}_2^{2+}/\text{PIPOH}$ system	19
VIII.	^1H NMR study of the $\text{UO}_2^{2+}/\text{NMAH}$ system	20
IX.	References	23

I. Crystallographic data for $[\text{UO}_2(\text{PIPO})_2(\text{H}_2\text{O})]$.

Table S1. Crystal data for $[\text{UO}_2(\text{PIPO})_2(\text{H}_2\text{O})]$.

CCDC	1579042
Formula	$\text{C}_{10}\text{H}_{18}\text{N}_2\text{O}_7\text{U}$
D_{calc} (g cm $^{-3}$)	2.458
μ (mm $^{-1}$)	11.669
Formula Weight	516.29
Colour / Shape	clear light red prisms
Size (mm 3)	0.40 × 0.30 × 0.17
T (K)	115(1)
Crystal System	monoclinic
Space Group	$P2_1/c$
a (Å)	6.472(3)
b (Å)	27.71(1)
c (Å)	8.310(3)
β ($^\circ$)	110.610(9)
V (Å 3)	1394.9(9)
Z	4
Z'	1
Wavelength (Å)	0.710730
Radiation type	Mo K α
$\Theta_{\text{min}} / \Theta_{\text{max}}$ ($^\circ$)	1.470 / 27.673
Measured / Independent / Used Reflections	31311 / 3243 / 3156
R_{int}	0.0412
Parameters	181
Restraints	0
Deepest Hole/Largest Peak	-2.351 / 2.013
GooF	1.309
wR_2 (all data)	0.0600
wR_2	0.0595
R_1 (all data)	0.0284
R_1	0.0273

Table S2. Hydrogen bond information for $[\text{UO}_2(\text{PIPO})_2(\text{H}_2\text{O})]$.^a

D	H	A	$d(\text{D}-\text{H})$ (Å)	$d(\text{H}\cdots\text{A})$ (Å)	$d(\text{D}\cdots\text{A})$ (Å)	$\text{D}-\text{H}\cdots\text{A}$ (°)
O4	H4A	O2 ¹	0.89	1.85	2.684(5)	153.6
O4	H4B	O2A ¹	0.89	1.85	2.656(5)	149.1

^a Symmetry transformations used to generate equivalent atoms: (1) $1 + x, y, z$.

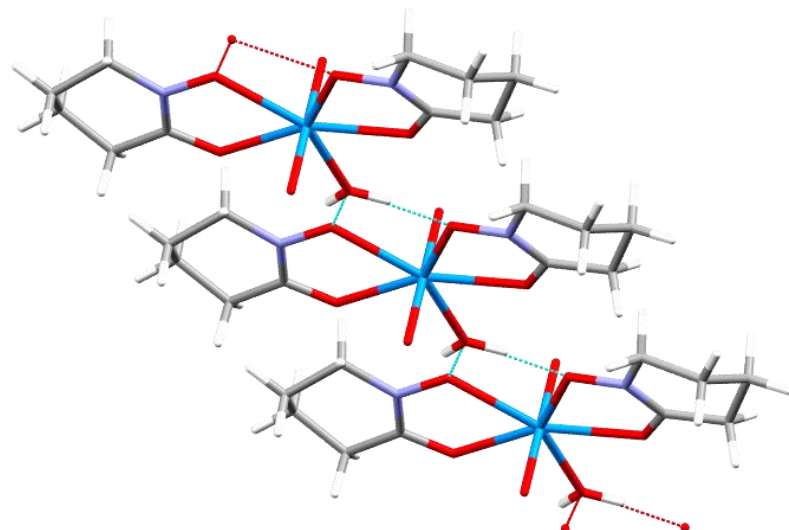


Table S3. Uranyl bond distances (\AA) and angles ($^\circ$) found in hydroxamato complexes. Structural data were retrieved from the CCDC database (release 5.38).

Complex	Ref. code	U=O	O=U=O	Ref.
[UO ₂ (NMA)(NO ₃)(H ₂ O) ₂]	QUKWOK	1.770(3) / 1.771(3)	176.7(1)	1
[UO ₂ (PBA)(THF) ₂ Cl]	CXBHFU	1.74(3) / 1.76(3)	180(1)	2
{[UO ₂ (FHA) ₂] _n }	ONETUY	1.779(6)	173.5(4)	3
{[UO ₂ (AHA) ₂] _n }	ISIYEP	1.766(5)	180	4
[UO ₂ (NMA) ₂ (H ₂ O)]	QUKWIE	1.783(4) / 1.786(4) ^a 1.788(4) / 1.782(4) ^a	176.9(2) ^a 177.7(2) ^a	1
[UO ₂ (PIPO) ₂ (H ₂ O)]	This work	1.783(4) / 1.778(4)	179.2(2)	^b
[UO ₂ (PBA) ₂ MeOH]	CIBHAW	1.75(1) / 1.75(1)	177.3(4)	5
[UO ₂ (PBA) ₂ DMF]	MUZWEK	1.77(1) / 1.79(1)	176.9(6)	6
[UO ₂ (PBA) ₂ DMSO]	CINRUN	1.773(4) / 1.781(4)	177.8(2)	7
{[UO ₂ (SHA) ₂]·2H ₂ O} _n	HIFNIU	1.769(6)	177.8(3)	8
[UO ₂ (IBPHA) ₂ (EtOH)]	PICNAQ	1.75	180	9

^a Two independent molecules crystallize in the asymmetric unit. ^b This work.

Table S4. U–O bond distances (\AA) and bite angles ($^\circ$) found in uranyl hydroxamato complexes. Structural data were retrieved from the CCDC database (release 5.38).

Complex	U–O _C	U–O _N	O _C –U–O _N	Ref.
[UO ₂ (NMA)(NO ₃)(H ₂ O) ₂]	2.396(3)	2.386(3)	64.3(1)	1
[UO ₂ (PBA)(THF) ₂ Cl]	2.34(3)	2.37(3)	67.0(1)	2
{[UO ₂ (FHA) ₂] _n }	2.450(6)	2.447(6)	64.4(2)	3
{[UO ₂ (AHA) ₂] _n }	2.432(5)	2.519(5)	62.4(2)	4
[UO ₂ (NMA) ₂ (H ₂ O)]	2.387(4) / 2.368(4) 2.371(4) / 2.384(4)	2.376(4) / 2.397(4) 2.402(4) / 2.377(4)	64.8(1) / 64.6(1) ^a 64.6(1) / 64.6(1) ^a	1
[UO ₂ (PIPO) ₂ (H ₂ O)]	2.365(4) / 2.376(4)	2.384(4) / 2.398(3)	66.1(1) / 65.5(1)	^b
[UO ₂ (PBA) ₂ MeOH]	2.40(1) / 2.35(1)	2.42(1) / 2.38(1)	64.9(2) / 65.5(3)	5
[UO ₂ (PBA) ₂ DMF]	2.365(8) / 2.396(9)	2.362(8) / 2.34(1)	65.4(3) / 64.8(3)	6
[UO ₂ (PBA) ₂ DMSO]	2.397(3) / 2.378(3)	2.341(3) / 2.367(3)	65.2(1) / 64.8(1)	7
{[UO ₂ (SHA) ₂]·2H ₂ O} _n	2.428(6)	2.464(5)	62.6(2)	8
[UO ₂ (IBPHA) ₂ (EtOH)]		2.38 ^d	n.r. ^c	9

^a Two independent molecules crystallize in the asymmetric unit. ^b This work. ^c The parameter is not reported and the coordinates are not available in the CSD. ^d Reported mean value.

Table S5. Selected bond distances (\AA) found in uranyl hydroxamato complexes. Structural data were retrieved from the CCDC database (release 5.38).

Complex	C=O	N–O	C–N	Ref.
[UO ₂ (NMA)(NO ₃)(H ₂ O) ₂]	1.332(5)	1.345(5)	1.289(6)	1
[UO ₂ (PBA)(THF) ₂ Cl]	1.44(4)	1.38(4)	1.24(5)	2
{[UO ₂ (FHA) ₂] _n }	1.28(1)	1.39(1)	1.29(1)	3
{[UO ₂ (AHA) ₂] _n }	1.288(8)	1.375(7)	1.300(9)	4
[UO ₂ (NMA) ₂ (H ₂ O)]	1.292(7) / 1.308(6) 1.303(6) / 1.294(7)	1.372(6) / 1.353(6) 1.360(6) / 1.362(6)	1.305(7) / 1.308(7) 1.297(7) / 1.311(7)	1
[UO ₂ (PIPO) ₂ (H ₂ O)]	1.317(6) / 1.303(6)	1.352(5) / 1.350(5)	1.308(6) / 1.309(6)	^b
[UO ₂ (PBA) ₂ MeOH]	1.27(1) / 1.34(1)	1.39(1) / 1.33(1)	1.32(1) / 1.28(2)	5
[UO ₂ (PBA) ₂ DMF]	1.28(1) / 1.305(9)	1.35(1) / 1.35(2)	1.29(2) / 1.31(1)	6
[UO ₂ (PBA) ₂ DMSO]	n.r. ^c	n.r. ^c	n.r. ^c	7
{[UO ₂ (SHA) ₂]·2H ₂ O} _n	1.28(1)	1.343(9)	1.31(1)	8
[UO ₂ (IBPHA) ₂ (EtOH)]	1.28 ^d	1.36 ^d	n.r. ^c	9

^a Two independent molecules crystallize in the asymmetric unit. ^b This work. ^c The parameter is not reported and the coordinates are not available in the CSD. ^d Reported mean value.

II. X-ray powder diffraction studies of uranyl complexes

Powder X-ray diffraction analyzes were carried out on an Empyrean diffractometer (Panalytical). The instrument was equipped with a copper anticathode tube ($\lambda = 1.54060 \text{ \AA}$ for $K_{\alpha 1}$ and 1.54443 \AA for $K_{\alpha 2}$) and a X'Celerator detector with anti-scatter slits of 5 mm. Diffractograms were recorded for $10 < 2\theta < 50^\circ$ in transmission mode by using a focusing X-ray mirror with divergence slits and anti-scatter slits (aperture 0.5°). Few milligrams of microcrystalline samples of $[\text{UO}_2(\text{NMA})_2(\text{H}_2\text{O})]$ and $[\text{UO}_2(\text{PIPO})_2(\text{H}_2\text{O})]$ that precipitated out at pH ~ 5 –6, were placed without being crushed between two Mylar sheets.

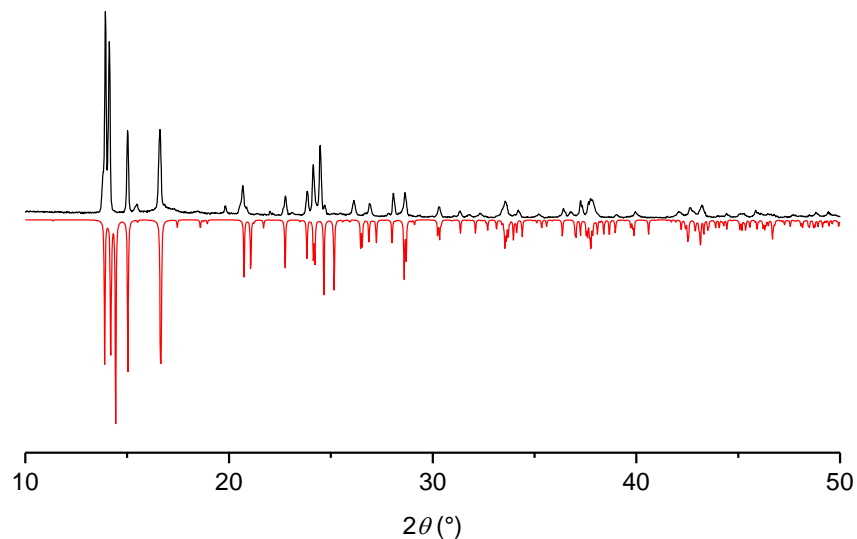


Figure S1. Experimental X-ray powder diffractogram ($T = 293 \text{ K}$) of microcrystalline $[\text{UO}_2(\text{NMA})_2(\text{H}_2\text{O})]$ precipitated at pH ~ 5 (black line). The red line shows the diffraction pattern calculated from the single-crystal data collected at $T = 100 \text{ K}$ (CCDC-1042608).

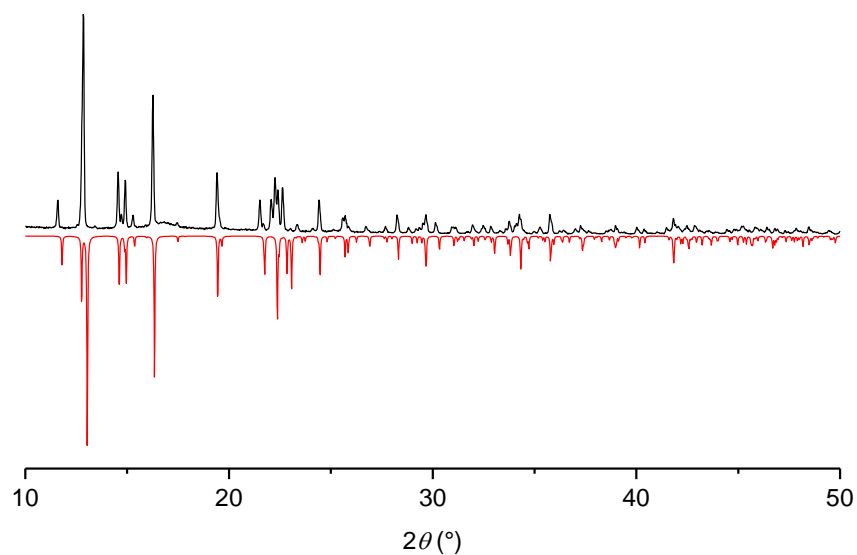


Figure S2. Experimental X-ray powder diffractogram ($T = 293 \text{ K}$) of microcrystalline $[\text{UO}_2(\text{PIPO})_2(\text{H}_2\text{O})]$ precipitated at pH ~ 6 (black line). The red line shows the diffraction pattern calculated from the single-crystal data collected at $T = 115 \text{ K}$ (CCDC-1579042).

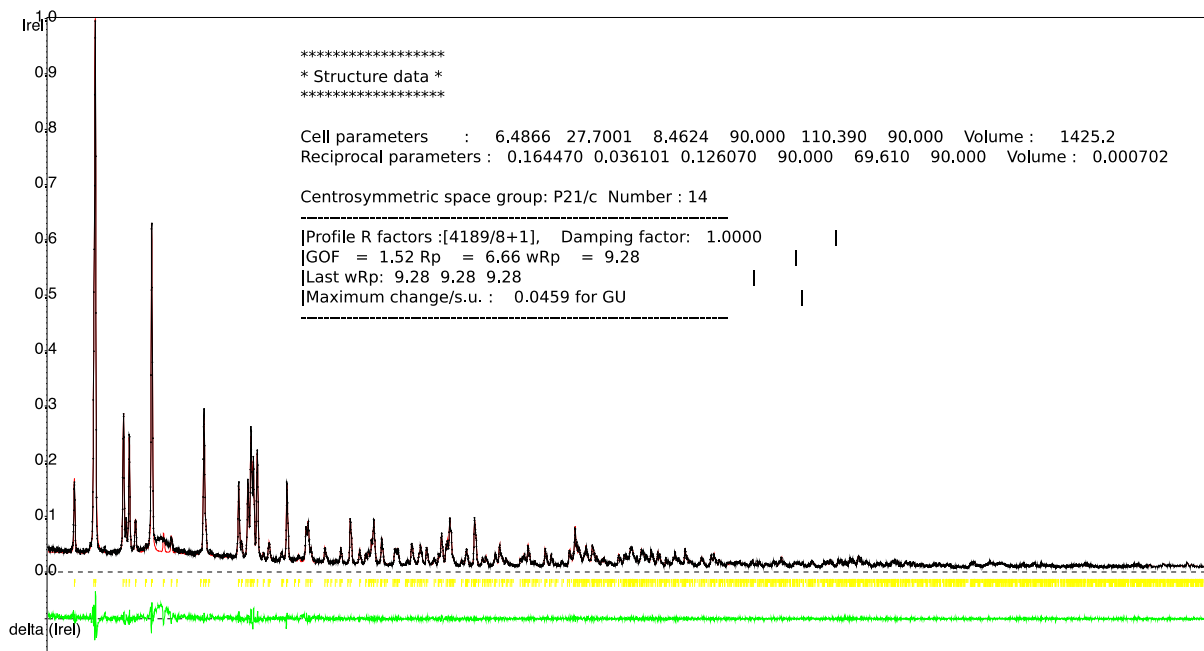


Figure S3. Experimental (black line) and refined (red line) X-ray powder diffractogram of microcrystalline $[\text{UO}_2(\text{PIPO})_2(\text{H}_2\text{O})]$ precipitated at pH ~ 6. Le Bail refinement¹⁰ in the $P\ 2_1/c$ space group was performed with the Jana Software.¹¹ Residues are plotted in green.

Table S6. Comparison of the cell parameters derived from the Le Bail refinement and the single crystal analysis for $[\text{UO}_2(\text{PIPO})_2(\text{H}_2\text{O})]$.

Cell parameters	Powder data ($T = 293\ \text{K}$) ^a	Single crystal data ($T = 115\ \text{K}$)
$a\ (\text{\AA})$	6.4866(1)	6.472(3)
$b\ (\text{\AA})$	27.7001(6)	27.71(1)
$c\ (\text{\AA})$	8.4624(2)	8.310(3)
$\beta\ (^{\circ})$	110.390(2)	110.610(9)

^a Other refined parameters: shift = 0.95(4), Gaussian $U = 18.23$, Gaussian $V = -0.893$, Gaussian $W = 5$, Lorentzian $L_x = 3.18$, $R_p = 6.66$, $wR_p = 9.28$.

III. Spectroscopic data of uranyl complexes

1. Diffuse reflectance spectroscopy

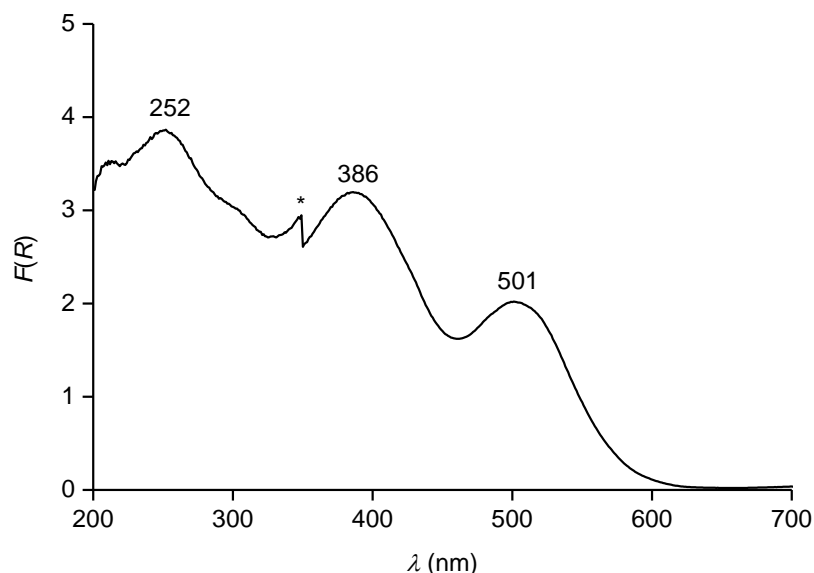


Figure S4. UV–vis diffuse reflectance spectrum of pure microcrystalline $[\text{UO}_2(\text{PIPO})_2(\text{H}_2\text{O})]$ precipitated at pH ~ 6. The full spectrum, recorded with a Praying Mantis (Harrick) accessory in the 200–2500 nm range, was truncated as no band was observed above 700 nm. The spectral artifact corresponding to the lamp change at 350 nm is marked with an asterisk.

2. Infrared spectroscopy

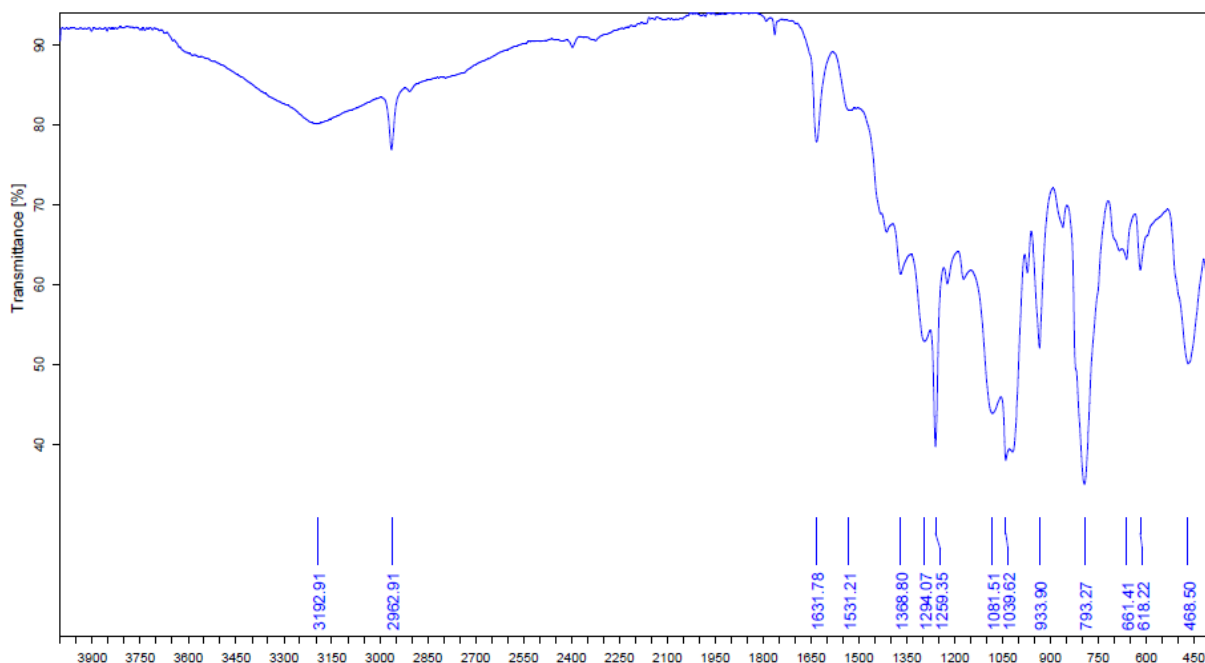


Figure S5. ATR FT-MIR spectrum of a $[\text{UO}_2(\text{NMA})(\text{NO}_3)(\text{H}_2\text{O})_2]$ single crystal.

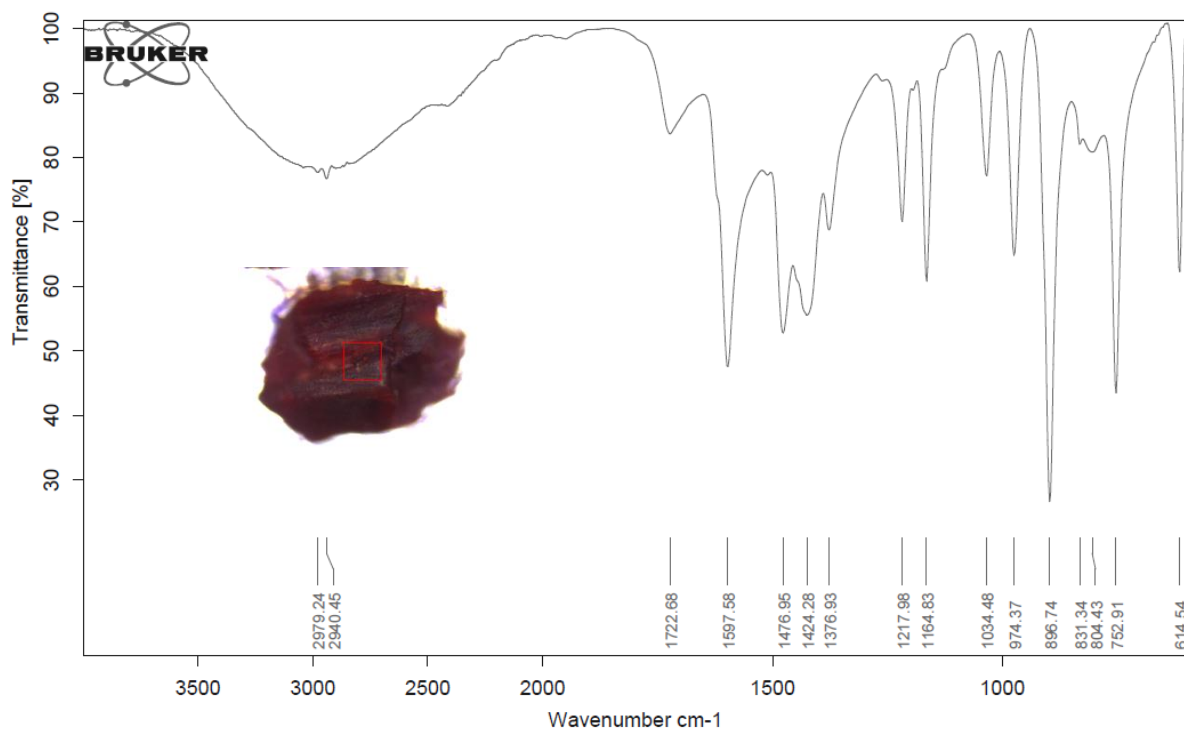


Figure S6. ATR FT-MIR spectrum of a $[\text{UO}_2(\text{NMA})_2(\text{H}_2\text{O})]$ single crystal.

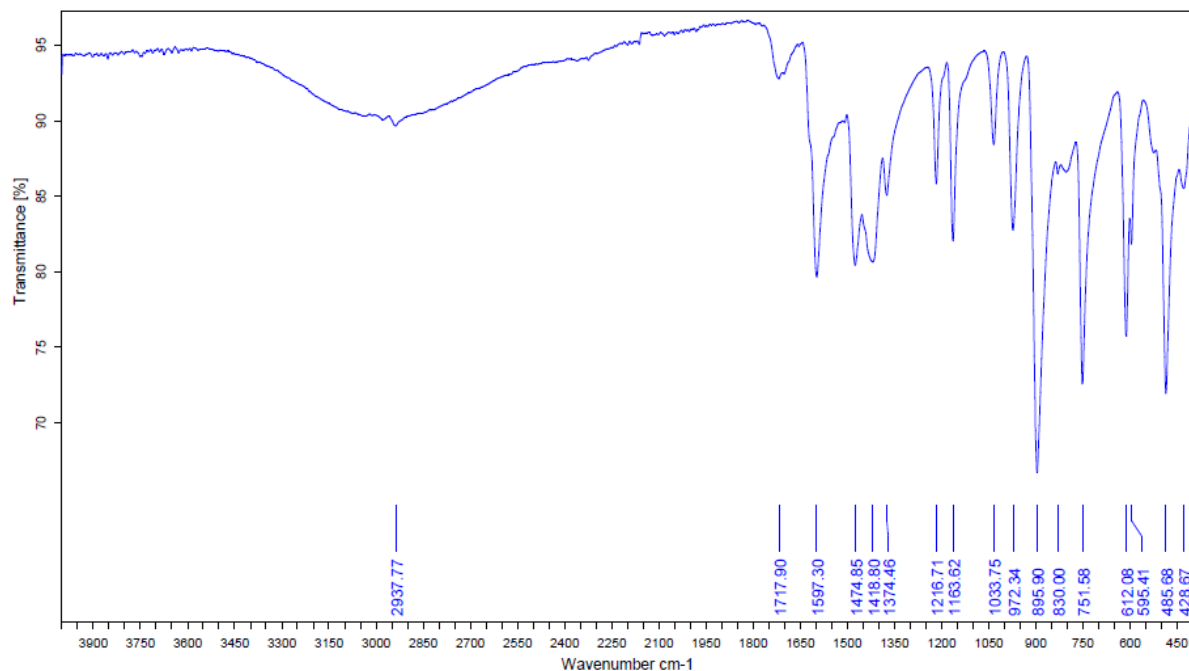


Figure S7. ATR FT-MIR spectrum of microcrystalline $[\text{UO}_2(\text{NMA})_2(\text{H}_2\text{O})]$ precipitated at pH ~ 5 .

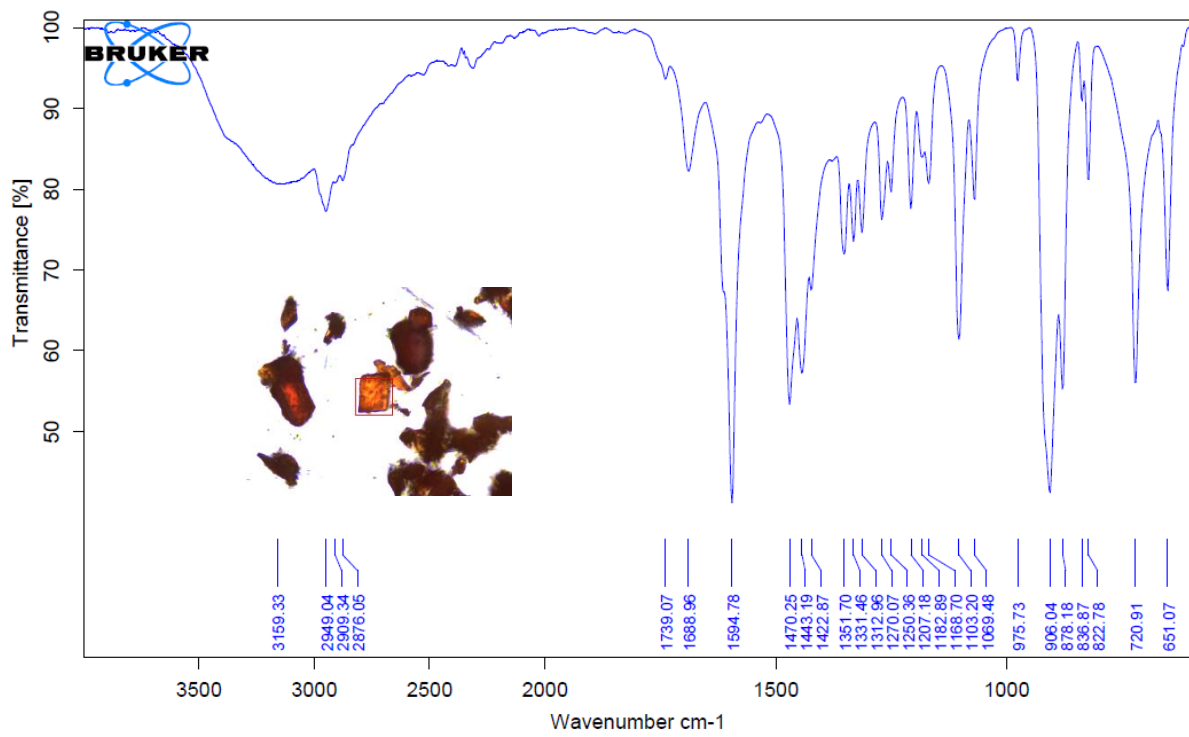


Figure S8. ATR FT-MIR spectrum of a $[\text{UO}_2(\text{PIPO})_2(\text{H}_2\text{O})]$ single crystal.

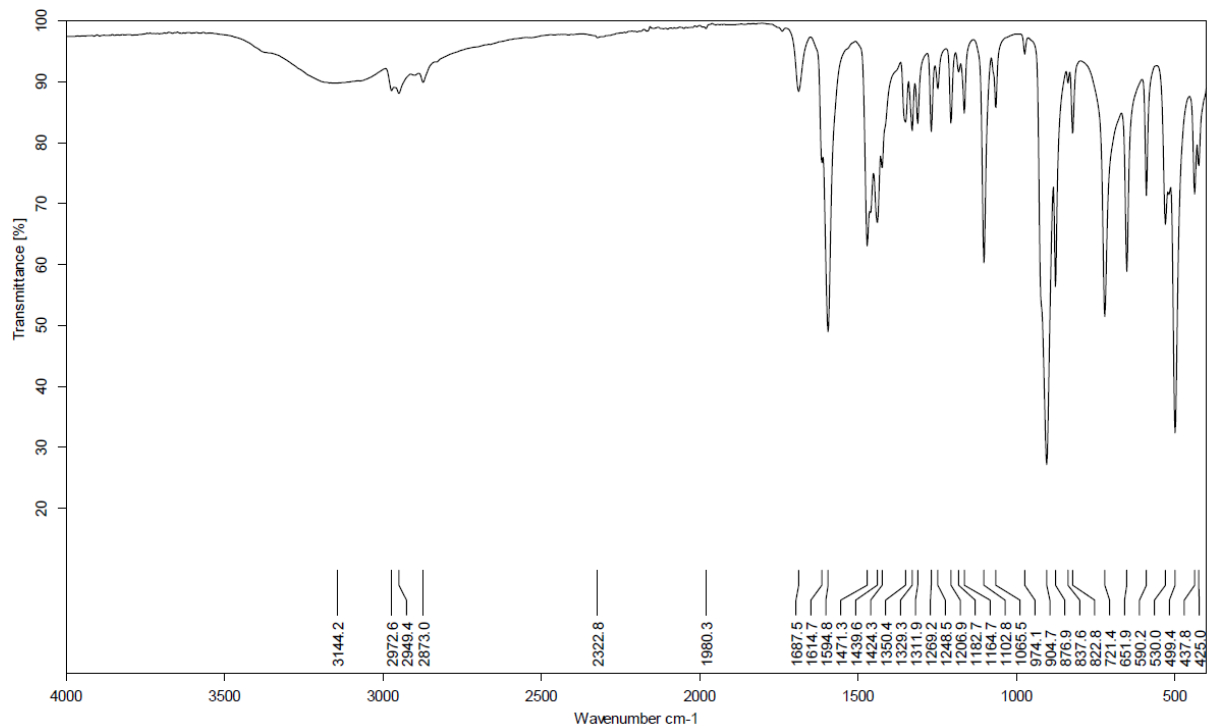


Figure S9. ATR FT-MIR spectrum of microcrystalline $[\text{UO}_2(\text{PIPO})_2(\text{H}_2\text{O})]$ precipitated at pH ~ 6 .

3. Raman spectroscopy

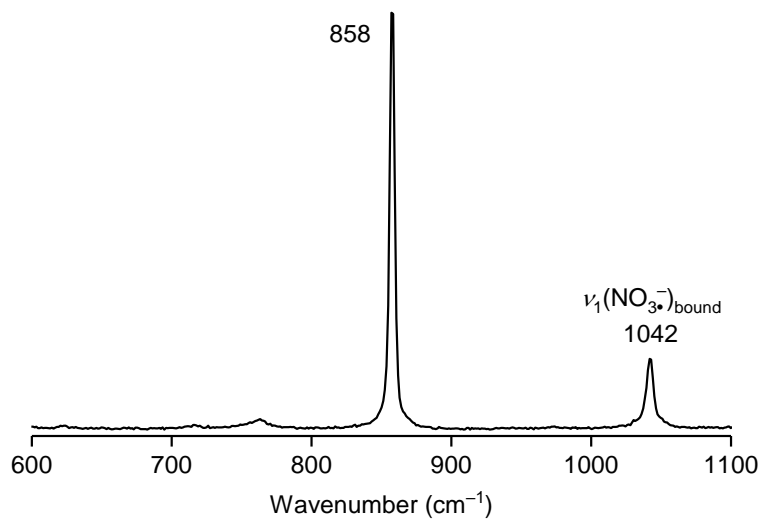


Figure S10. Raman spectrum of $[\text{UO}_2(\text{NMA})(\text{NO}_3)(\text{H}_2\text{O})_2]$ single crystals. $\lambda_{\text{exc}} = 633 \text{ nm}$.

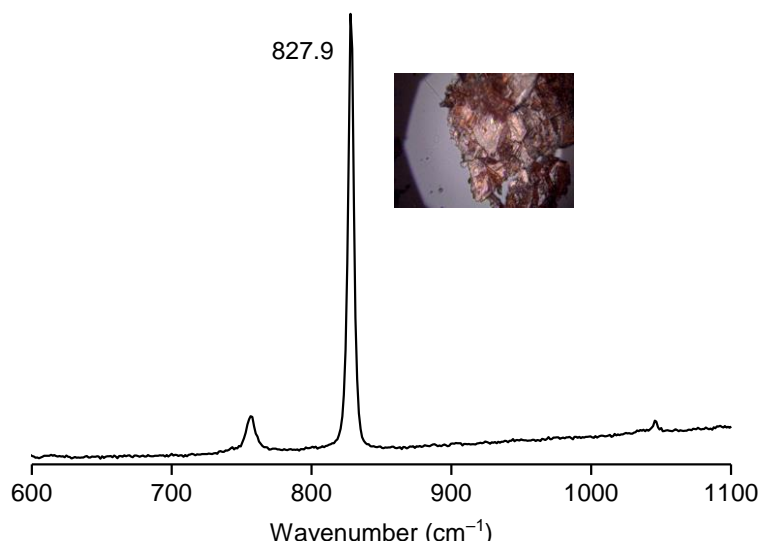


Figure S11. Raman spectrum of $[\text{UO}_2(\text{NMA})_2(\text{H}_2\text{O})]$ crystals. $\lambda_{\text{exc}} = 633 \text{ nm}$.

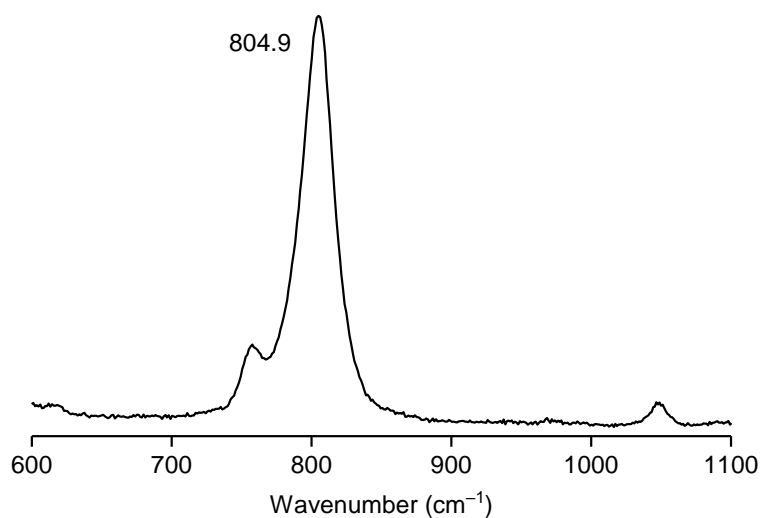


Figure S12. Raman spectrum of a solid sample of $\text{K}[\text{UO}_2(\text{NMA})_2(\text{OH})]$ isolated at pH 9.6. $\lambda_{\text{exc}} = 785 \text{ nm}$.

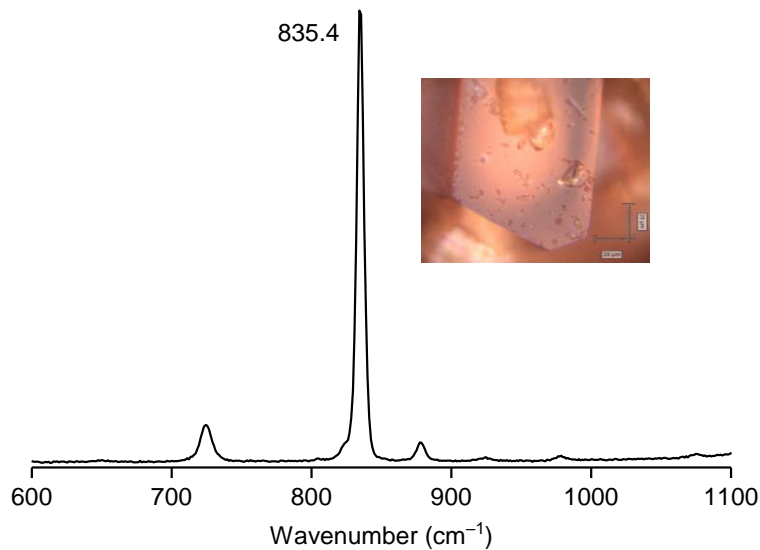


Figure S13. Raman spectrum of a $[\text{UO}_2(\text{PIPO})_2(\text{H}_2\text{O})]$ single crystal.

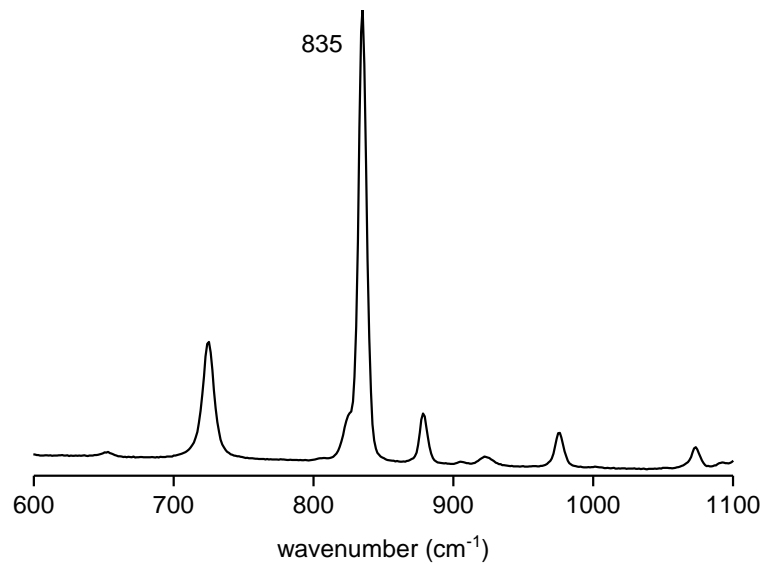


Figure S14. Raman spectrum of microcrystalline $[\text{UO}_2(\text{PIPO})_2(\text{H}_2\text{O})]$ precipitated at $\text{pH} \sim 6$.

IV. Protonation constants of NMA^-

Table S7. Literature survey of the protonation constant values of *N*-methylacetohydroxamate (NMA^-).

$\log K_{011}$	I (M)	Medium	T (K)	Method ^a	Calib. pH ^b	Ref
8.95(7)	0.1	NaClO_4	298.15	UV-vis	conc.	12
8.80	0.1	NaNO_3	298.15	Pot.	conc.	13
8.75	0.1	KNO_3	298.15	Pot.	conc.	14
8.63(1)	0.2	KCl	298.15	Pot.	conc.	15-16
8.67(3)	0.2	KCl	298.15	Pot.	conc.	17
8.69(1)	0.2	KCl	298.15	Pot.	conc.	18
8.70(1)	0.2	KCl	298.15	Pot.	conc.	19-21
8.67(1)	0.2	KNO_3	298.15	Pot.	conc.	22
8.63(1)	2.0	NaClO_4	298.15	Pot.	buffers	23
8.95(3)	2.0	NaClO_4	298.15	Pot.	conc.	24-25

^a Method used: glass-electrode potentiometry (Pot.), absorption spectrophotometry (UV-vis).

^b Calibration of the pH electrode by means of strong acid/base titrations (conc.) or buffers (buffers). In the latter case, K_{011} corresponds to a mixed conditional protonation constant defined as $K_{011} = [\text{LH}] / \{[\text{L}^-] a_{\text{H}}\}$, where a_{H} stands for the free proton activity.

V. Isothermal titration calorimetric study of the protonation of NMA^- and PIPO^-

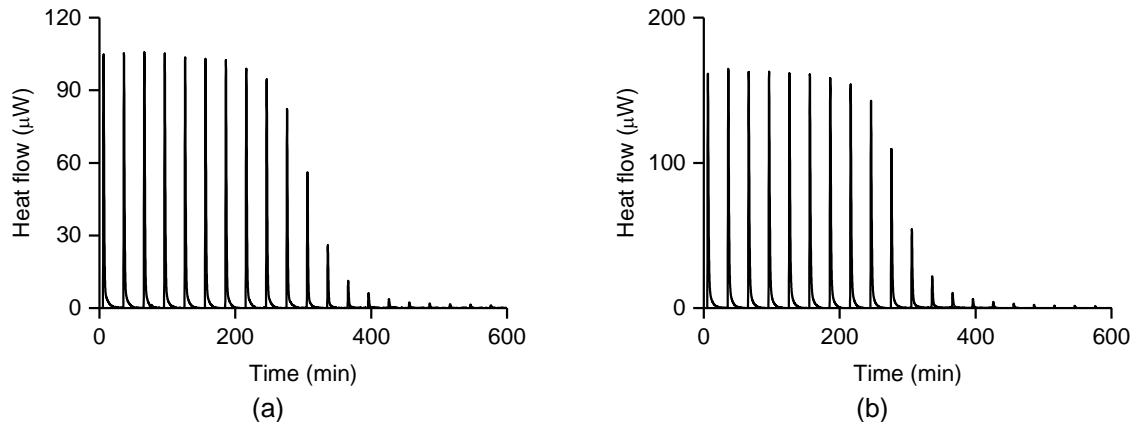


Figure S15. Thermograms corresponding to the neutralization of NMAH (a) and PIPOH (b) with KOH added every 30 min in 5 μL increments. $I = 0.1 \text{ M KNO}_3$, $T = 298.15 \text{ K}$, $V_0 = 0.800 \text{ mL}$. (a) $[\text{NMAH}]_{\text{tot}} = 3.34 \text{ mM}$, $[\text{KOH}] = 0.04986 \text{ M}$. (b) $[\text{NMAH}]_{\text{tot}} = 6.34 \text{ mM}$, $[\text{KOH}] = 0.0998 \text{ M}$.

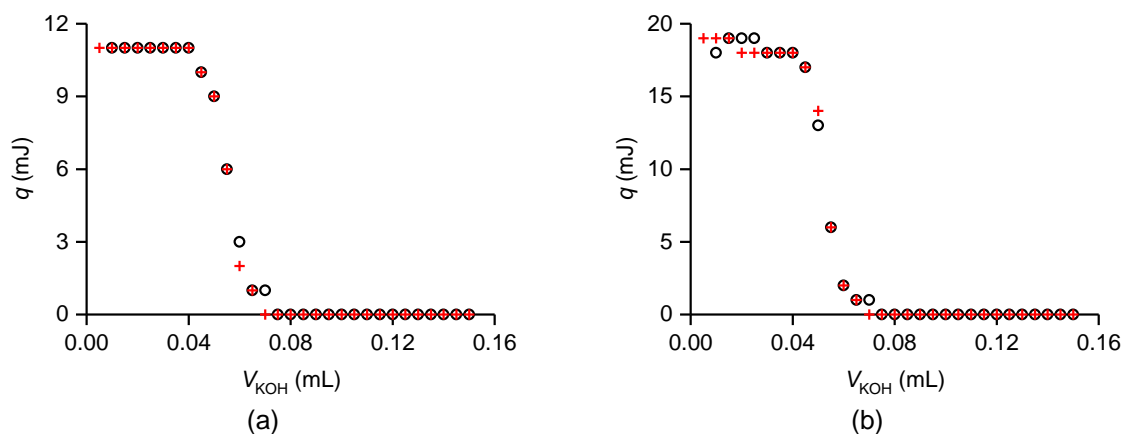
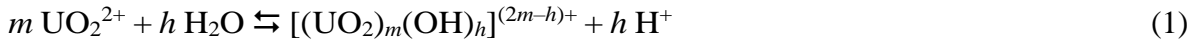


Figure S16. Integrated heats corrected for dilution effects (open circles) corresponding to the neutralization of NMAH (a) and PIPOH (b). $I = 0.1 \text{ M KNO}_3$, $T = 298.15 \text{ K}$. The red crosses correspond to the nonlinear least-squares fit of the data by the Hypcal program.²⁶

VI. Hydrolysis constants of UO_2^{2+}

Hydrolysis constants for UO_2^{2+} (eqn (1)) at infinite dilution (β_{m0-h}^0 , eqn (2)) were retrieved from the critical compilation of Guillaumont et al. and corrected for medium effects by applying the specific ion interaction theory (SIT) (eqn (3)).²⁷



$$\log \beta_{m0-h}^0 = \frac{[(\text{UO}_2)_m(\text{OH})_h] [\text{H}]^h}{[\text{UO}_2]^m a_w^h} \quad (2)$$

$$\log \beta_{m0-h}^{\text{molal}} = \log \beta_{m0-h}^0 + \Delta z^2 D + m \log a_w - \Delta \epsilon I_m \quad (3)$$

where:

$$\Delta z^2 = (2m - h)^2 + h - 4m \quad (4)$$

$$D = \frac{0.509 \sqrt{I_m}}{1 + 1.5 \sqrt{I_m}} \quad (5)$$

The molar ionic strength ($I = 0.1 \text{ M KNO}_3$) was converted into the molal scale ($I_m = 0.10069 \text{ mol kg}^{-1}$) by considering a density of $\rho = 1.0032 \text{ g cm}^3$ at 298.15 K.²⁸ Under such conditions, $D = 0.10943$.

$$\log a_w = -0.015648 \phi I_m \quad (6)$$

The water activity (a_w) of the supporting electrolyte solution was calculated by eqn (6) in which ϕ is the osmotic coefficient. Values of ϕ tabulated by Robison and Stokes²⁹ for KNO_3 solutions were interpolated with the help of the relation proposed by Hamer and Wu and recommended by NIST (eqn (7)).³⁰

$$\begin{aligned} \phi = 1 - \frac{0.509 \ln 10}{a^3 I_m} & \left\{ (1 + a \sqrt{I_m}) - 2 \ln (1 + a \sqrt{I_m}) - (1 + a \sqrt{I_m})^{-1} \right\} \\ & + \frac{1}{2} b I_m + \frac{2}{3} c I_m^2 + \frac{3}{4} d I_m^3 \end{aligned} \quad (7)$$

The four empirical parameters a , b , c , and d of eqn (7) were adjusted by unweighted non-linear least-squares fitting, yielding $a = 0.85(1)$, $b = -0.200(4)$, $c = 0.0111(6)$, and $d = 0$. Accordingly, the values of $\phi = 0.9037$ and $a_w = 0.9967$ were obtained for a 0.1 M KNO_3 solution.

$$\Delta \epsilon = \epsilon([(\text{UO}_2)_m(\text{OH})_h]^{(2m-h)+}, \text{NO}_3^- \text{ or } \text{Na}^+) + h \epsilon(\text{H}^+, \text{NO}_3^-) - m \epsilon(\text{UO}_2^{2+}, \text{ClO}_4^-) \quad (8)$$

The ion interaction coefficients of eqn (8) were taken from the review of Guillaumont et al.²⁷ and are listed as $\Delta\epsilon$ values in Table S8, with $\epsilon(H^+, NO_3^-) = 0.07(1) \text{ kg mol}^{-1}$ and $\epsilon(H^+, ClO_4^-) = 0.46(3) \text{ kg mol}^{-1}$. As no $\Delta\epsilon$ coefficient has been reported for $[UO_2(OH)_4]^{2-}$, $[(UO_2)_2(OH)]^{3+}$, $[(UO_2)_3(OH)_7]^-$, and $[(UO_2)_4(OH)_7]^+$, this parameter has been arbitrarily set to 0 for these species. At $I = 0.1 \text{ M}$, this assumption has no major influence on the final outcome.

The thus calculated $\log \beta_{m0-h}^{\text{molal}}$ values expressed in the molal scale were then converted into molar equilibrium constants by eqn (9).

$$\log \beta_{m0-h}^c = \log \beta_{m0-h}^{\text{molal}} - (1-m) \log \left(\frac{I_m}{I} \right) \quad (9)$$

Finally, the conditional equilibrium constants β_{m0-h} , which take into account the formation of the weak $[UO_2(NO_3)]^+$ complex in nitrate media, were derived by applying eqn (10).³¹ The $\log \beta_{m0-h}$ values compiled in the last column of Table S8 were considered in all speciation calculations.

$$\log \beta_{m0-h} = \log \beta_{m0-h}^c - m \log \alpha_U \quad (10)$$

$$\text{with } \alpha_U = 1 + \beta_{[UO_2(NO_3)]^+} [NO_3^-] \quad (11)$$

$\beta_{[UO_2(NO_3)]^+}$ was estimated by the SIT approach from the value reported at infinite dilution by Grenthe et al. ($\log \beta_{[UO_2(NO_3)]^+}^0 = 0.30 \pm 0.15$) and $\epsilon([UO_2(NO_3)]^+, ClO_4^-) = 0.33 \pm 0.04 \text{ kg mol}^{-1}$.³¹ For $I = 0.1 \text{ M KNO}_3$, we found $\log \beta_{[UO_2(NO_3)]^+} = -0.14 \pm 0.15$, yielding $\log \alpha_U = 0.03 \pm 0.01$.

Table S8. Hydrolysis constants for UO_2^{2+} at $I = 0$ (β_{m0-h}^0)³¹ and 0.1 M KNO_3 (β_{m0-h}) estimated by the specific ion interaction theory (SIT).

Species	$\log \beta_{m0-h}^0$	$\Delta\epsilon (\text{kg mol}^{-1})$	$\log \beta_{m0-h}^c$	$\log \beta_{m0-h}$
$[UO_2(OH)]^+$	-5.25 ± 0.24	0.12 ± 1.4	-5.5 ± 0.5	-5.5 ± 0.5
$[UO_2(OH)_2]$	-12.15 ± 0.07	-0.32 ± 0.04	-12.34 ± 0.07	-12.37 ± 0.07
$[UO_2(OH)_3]^-$	-20.25 ± 0.42	-0.34 ± 0.07	-20.2 ± 0.4	-20.3 ± 0.4
$[UO_2(OH)_4]^{2-}$	-32.40 ± 0.68	n.r.	-32 ± 1	-32 ± 1
$[(UO_2)_2(OH)]^{3+}$	-2.7 ± 1.0	n.r.	-2.5 ± 1.0	-2.5 ± 1.0
$[(UO_2)_2(OH)_2]^{2+}$	-5.62 ± 0.04	-0.29 ± 0.11	-5.81 ± 0.05	-5.87 ± 0.05
$[(UO_2)_3(OH)_4]^{2+}$	-11.9 ± 0.3	-0.38 ± 1.00	-12.3 ± 0.4	-12.4 ± 0.4
$[(UO_2)_3(OH)_5]^+$	-15.55 ± 0.12	-0.62 ± 0.24	-16.2 ± 0.1	-16.2 ± 0.1
$[(UO_2)_3(OH)_7]^-$	-32.2 ± 0.8	n.r.	-32.6 ± 1.0	-32.7 ± 1.0
$[(UO_2)_4(OH)_7]^+$	-21.9 ± 1.0	n.r.	-22.8 ± 1.0	-22.9 ± 1.0

VII. Affinity capillary electrophoretic study of the UO_2^{2+} /PIPOH system

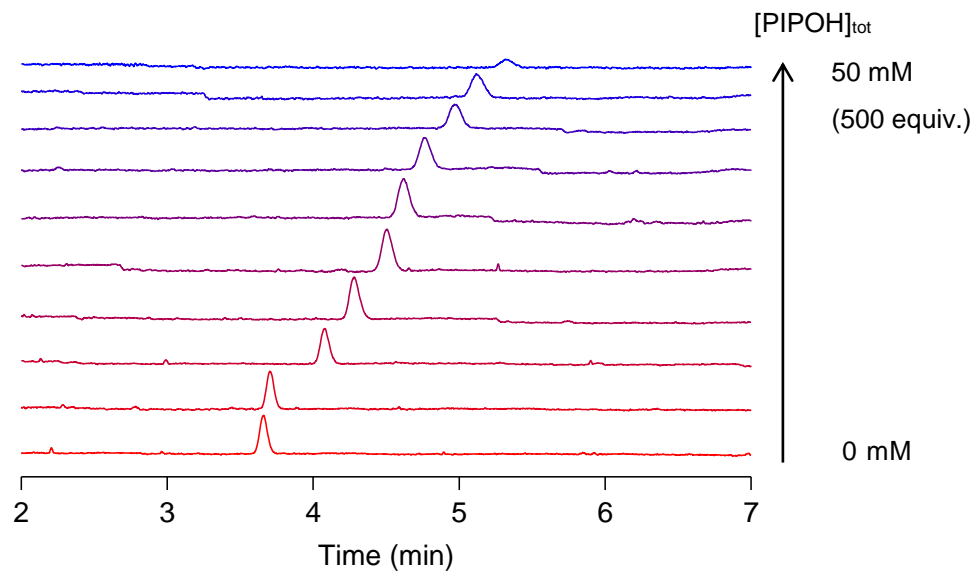


Figure S17. Affinity capillary electrophoregrams recorded for the UO_2^{2+} /PIPOH system as a function of the total ligand concentration in the background electrolyte. $I = 0.1 \text{ M} (\text{H},\text{Na})\text{ClO}_4$, $p[\text{H}] = 2.50(5)$, $T = 298.2(5) \text{ K}$, $[\text{U(VI)}]_{\text{tot}} = 0.1 \text{ mM}$, $[\text{PIPOH}]_{\text{tot}} = 0, 0.5, 2.5, 5, 8, 10, 15, 25, 30, 50 \text{ mM}$ (curve 1–10, 0–500 equiv.), $t_{\text{inj}} = 4 \text{ s}$, $\Delta P_{\text{inj}} = 0.5 \text{ psi}$, $V = 5 \text{ kV}$, capillary: $L = 31.2 \text{ cm}$, $L_{\text{det}} = 21 \text{ cm}$, $\varnothing_{\text{int}} = 50 \mu\text{m}$, UV-detector ($\lambda = 200 \text{ nm}$).

VIII. ^1H NMR study of the $\text{UO}_2^{2+}/\text{NMAH}$ system

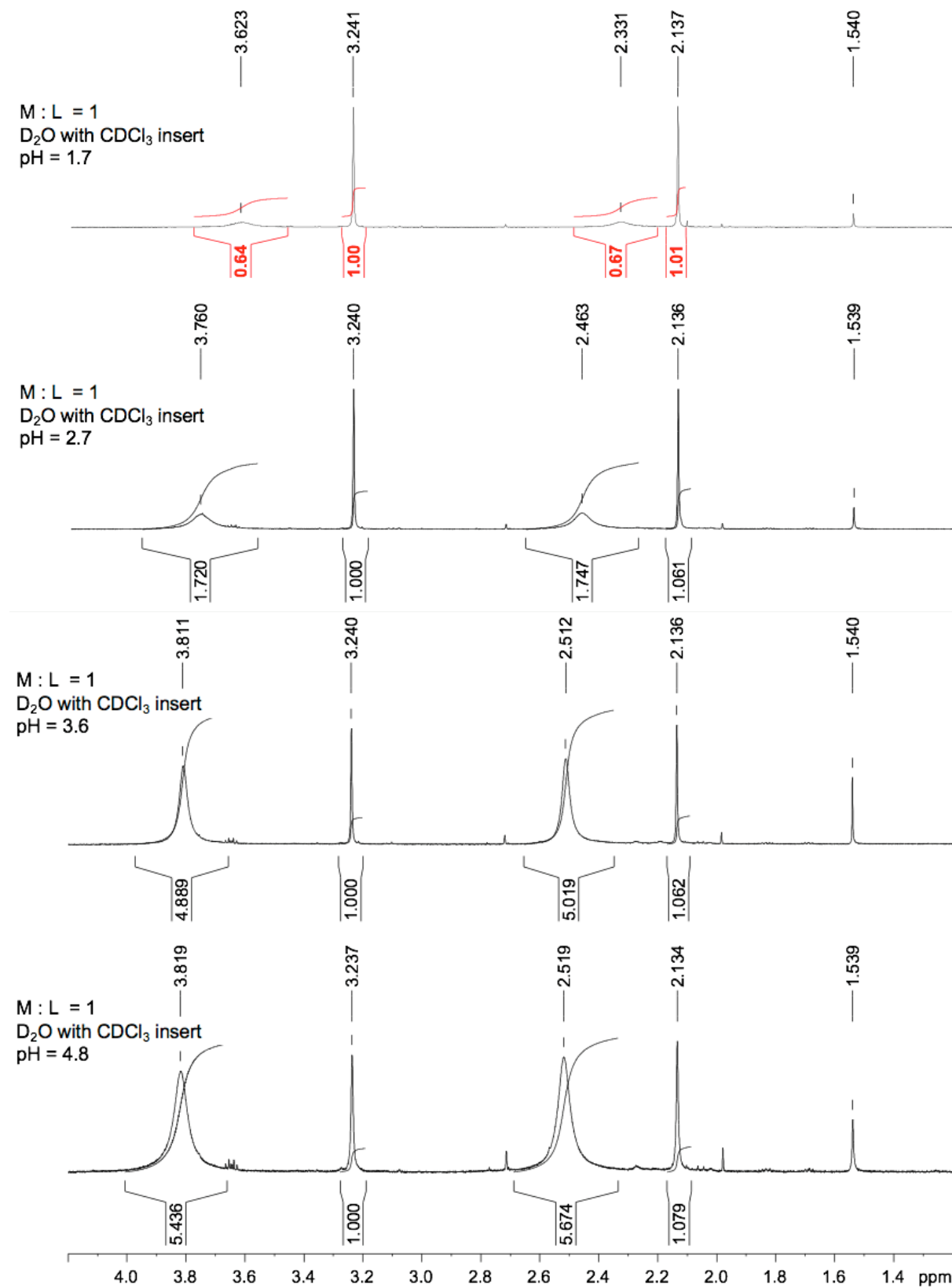


Figure S18. ^1H NMR spectra recorded for the $\text{UO}_2^{2+}/\text{NMAH}$ system in D_2O at different pH values for a 1:1 metal-over ligand concentration ratio. $[\text{U(VI)}]_{\text{tot}} = [\text{NMAH}]_{\text{tot}} = 26.8 \text{ mM}$, 600 MHz, $T = 300 \text{ K}$.

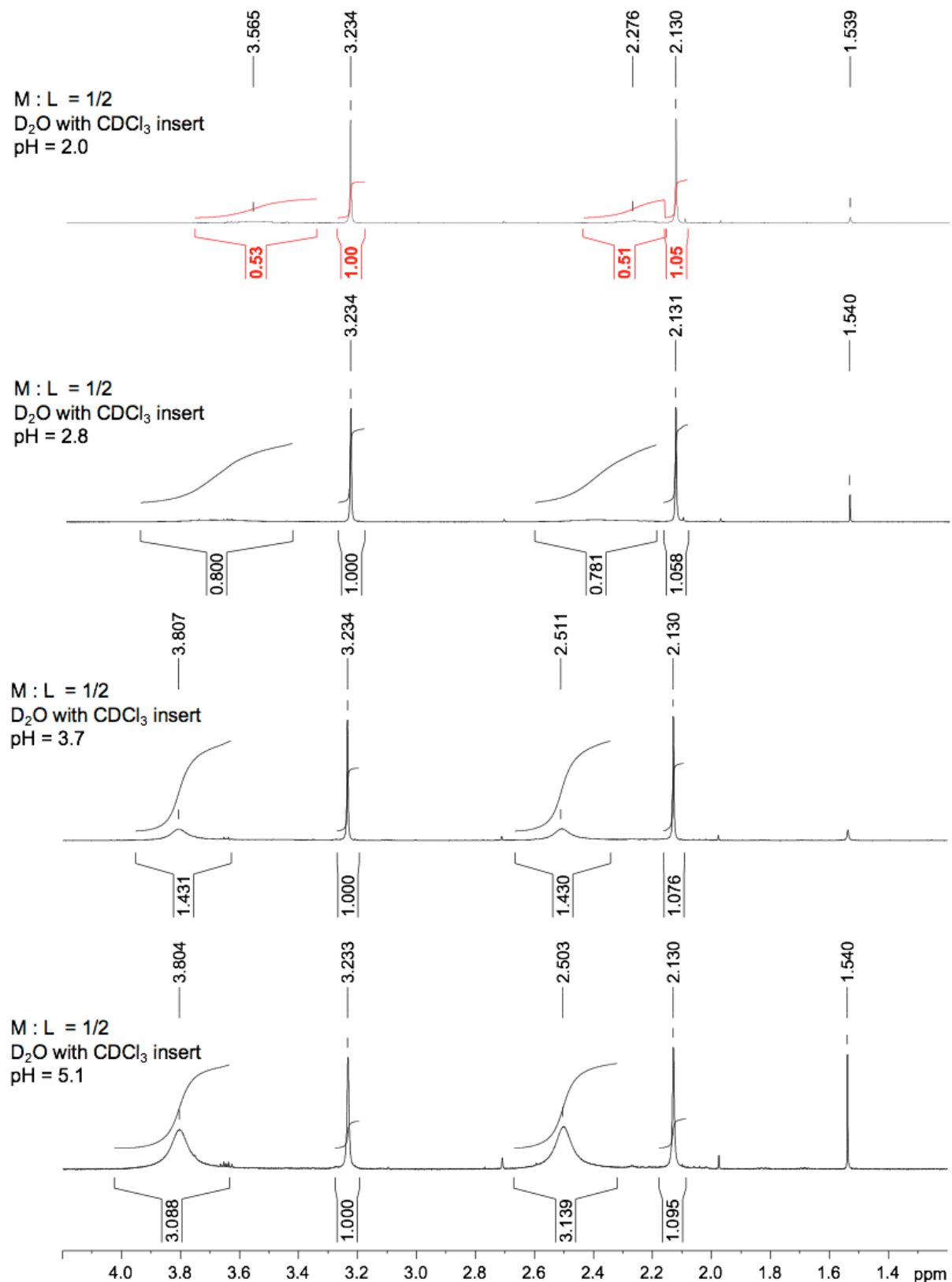
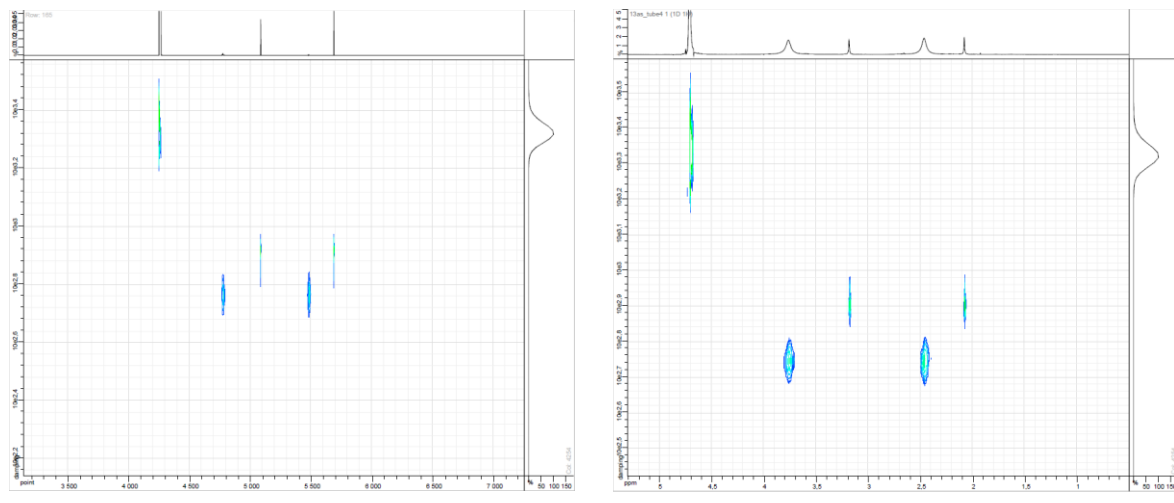


Figure S19. ¹H NMR spectra recorded for the UO₂²⁺/NMAH system in D₂O at different pH values for a 1:2 metal-over ligand concentration ratio. [U(VI)]_{tot} = 13.4 mm, [NMAH]_{tot} = 26.8 mM, 600 MHz, T = 300 K.

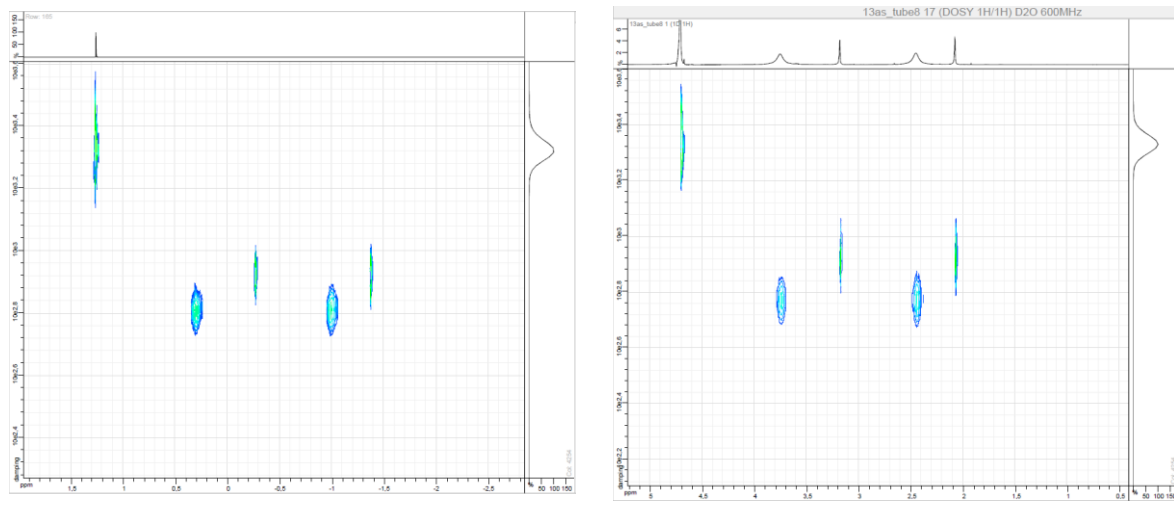
$$[\text{U(VI)}]_{\text{tot}} = [\text{NMAH}]_{\text{tot}} = 26.8 \text{ mM}$$



pH = 3.6

pH = 4.8

$$[\text{U(VI)}]_{\text{tot}} = 13.4 \text{ mM}, [\text{NMAH}]_{\text{tot}} = 26.8 \text{ mM}$$



pH = 3.7

pH = 5.2

Figure S20. ¹H NMR DOSY spectra recorded for the $\text{UO}_2^{2+}/\text{NMAH}$ system in D_2O at different metal-over ligand concentration ratios and pH values. 600 MHz, $T = 300 \text{ K}$.

IX. References

- 1 P. Jewula, J.-C. Berthet, J.-C. Chambron, Y. Rousselin, P. Thuéry and M. Meyer, *Eur. J. Inorg. Chem.*, 2015, 1529-1541.
- 2 W. L. Smith and K. N. Raymond, *J. Inorg. Nucl. Chem.*, 1979, **41**, 1431-1436.
- 3 M. A. Silver, W. L. Dorfner, S. K. Cary, J. N. Cross, J. Lin, E. J. Schelter and T. E. Albrecht-Schmitt, *Inorg. Chem.*, 2015, **54**, 5280-5284.
- 4 P. F. Weck, C.-M. S. Gong, E. Kim, P. Thuéry and K. R. Czerwinski, *Dalton Trans.*, 2011, **40**, 6007-6011.
- 5 U. Casellato, P. A. Vigato, S. Tamburini, R. Graziani and M. Vidali, *Inorg. Chim. Acta*, 1984, **81**, 47-54.
- 6 D. K. Hazra, S. Dinda, M. Helliwell, R. Bhattacharyya and M. Mukherjee, *Z. Kristallogr.*, 2009, **224**, 544-550.
- 7 S. Chakraborty, S. Dinda, R. Bhattacharyya and A. K. Mukherjee, *Z. Kristallogr.*, 2006, **221**, 606-611.
- 8 R. Centore, G. De Tommaso, M. Iuliano and A. Tuzi, *Acta Crystallogr., Sect. C*, 2007, **63**, m253-m255.
- 9 M. Hojjatie, S. Muralidharan, P. S. Bag, C. G. Panda and H. Freiser, *Iran. J. Chem. Eng.*, 1995, **14**, 81-89.
- 10 A. Le Bail, H. Duroy and J. L. Fourquet, *Mater. Res. Bull.*, 1988, **23**, 447-452.
- 11 V. Petříček, M. Dušek and L. Palatinus, *Z. Kristallogr. - Cryst. Mater.*, 2014, **229**, 345-352.
- 12 M. Biruš, A. Budimir and M. Gabričević, *J. Inorg. Biochem.*, 1999, **75**, 85-91.
- 13 A. E. Fazary, *J. Chem. Eng. Data*, 2005, **50**, 888-895.
- 14 F. Guérard, Y.-S. Lee, R. Tripier, L. P. Szajek, J. R. Deschamps and M. W. Brechbiel, *Chem. Commun.*, 2013, **49**, 1002-1004.
- 15 E. Farkas and O. Szabó, *Inorg. Chim. Acta*, 2012, **392**, 354-361.
- 16 O. Szabó and E. Farkas, *Inorg. Chim. Acta*, 2011, **376**, 500-508.
- 17 J. Comiskey, E. Farkas, K. A. Krot-Lacina, R. G. Pritchard, C. A. McAuliffe and K. B. Nolan, *Dalton Trans.*, 2003, 4243-4249.
- 18 P. Buglyó and N. Pótári, *Polyhedron*, 2005, **24**, 837-845.
- 19 E. Farkas, E. Kozma, M. Petho, K. M. Herlihy and G. Micera, *Polyhedron*, 1998, **17**, 3331-3342.
- 20 E. Farkas, É. A. Enyedy and H. Csóka, *J. Inorg. Biochem.*, 2000, **79**, 205-211.
- 21 E. Farkas, É. A. Enyedy, G. Micera and E. Garribba, *Polyhedron*, 2000, **19**, 1727-1736.
- 22 P. Buglyó, K. Lénárt, M. Kozsup, A. C. Bényei, É. Kováts, I. Sóvágó and E. Farkas, *Polyhedron*, 2015, **100**, 392-399.
- 23 B. Monzyk and A. L. Crumbliss, *J. Org. Chem.*, 1980, **45**, 4670-4675.
- 24 M. T. Caudle and A. L. Crumbliss, *Inorg. Chem.*, 1994, **33**, 4077-4085.
- 25 M. T. Caudle, C. D. Caldwell and A. L. Crumbliss, *Inorg. Chim. Acta*, 1995, **240**, 519-525.
- 26 G. Arena, P. Gans and C. Sgarlata, *Anal. Bioanal. Chem.*, 2016, **408**, 6413-6422.
- 27 R. Guillaumont, T. Fanghänel, J. Fuger, I. Grenthe, V. Neck, D. A. Palmer and M. H. Rand, *Update on the Chemical Thermodynamics of Uranium, Neptunium, Plutonium, Americium and Technetium*, Elsevier, Amsterdam, 2003.

- 28 O. Söhnel and P. Novotny, *Densities of Aqueous Solutions of Inorganic Substances*, Elsevier, Amsterdam, 1985.
- 29 R. A. Robinson and R. H. Stokes, *Electrolyte Solutions*, 2nd edn., Butterworths Scientific Publications, London, 1959.
- 30 W. J. Hamer and Y. C. Wu, *J. Phys. Chem. Ref. Data*, 1972, **1**, 1047-1099.
- 31 I. Grenthe, J. Fuger, R. J. M. Konings, R. J. Lemire, A. B. Muller, C. Nguyen-Trung and H. Wanner, *Chemical Thermodynamics of Uranium*, 2nd edn., OECD Nuclear Energy Agency, Paris, 2004.